Site of vulnerability on SARS-CoV-2 spike induces broadly protective antibody to antigenically distinct Omicron subvariants

Siriruk Changrob[1,15], Peter J. Halfmann[2,15], Hejun Liu[3,15], Jonathan L. Torres[3,15], Joshua J.C. McGrath[1], Gabriel Ozorowski[3], Lei Li[1], G. Dewey Wilbanks[1], Makoto Kuroda[2], Tadashi Maemura[2], Min Huang[1], Nai-Ying Zheng[1], Hannah L. Turner[3], Steven A. Erickson[4], Yanbin Fu[1], Atsuhiro Yasuhara[1], Gagandeep Singh[5,6], Brian Monahan[6,7], Jacob Mauldin[6,7], Komal Srivastava[6,7], Viviana Simon[5,6,7,8,9], Florian Krammer[5,6,7], D. Noah Sather[10], Andrew B. Ward[3], Ian A. Wilson[3,11], Yoshihiro Kawaoka[2,12,13,14], Patrick C. Wilson[1, 16*]

Affiliations:

[1] Drukier Institute for Children's Health, Department of Pediatrics, Weill Cornell Medicine, New York, NY 10021, USA.

[2] Influenza Research Institute, Department of Pathobiological Sciences, School of Veterinary Medicine, University of Wisconsin-Madison, Madison, WI 53711, USA.

[3] Department of Integrative Structural and Computational Biology, The Scripps Research Institute, La Jolla, CA 92037, USA.

[4] University of Chicago Department of Medicine, Section of Rheumatology, Chicago, IL 60637, USA.

[5] Department of Pathology, Molecular and Cell Based Medicine, Icahn School of Medicine at Mount Sinai, New York, NY 10029, USA.

[6] Department of Microbiology, Icahn School of Medicine at Mount Sinai, New York, NY 10029, USA.

[7] Center for Vaccine Research and Pandemic Preparedness, Icahn School of Medicine at Mount Sinai, New York, NY, 10029 USA.

[8] The Global Health and Emerging Pathogens Institute, Icahn School of Medicine at Mount Sinai, New York, NY, 10029 USA.

[9] Division of Infectious Diseases, Department of Medicine, Icahn School of Medicine at Mount Sinai, New York, NY 10029, USA.

[10] Center for Global Infectious Disease Research, Seattle Children's Research Institute, Seattle, WA 98101, USA; Department of Pediatrics, University of Washington, Seattle, Washington, USA; Department of Global Health, University of Washington, Seattle, WA 98105, USA.

[11] The Skaggs Institute for Chemical Biology, The Scripps Research Institute; La Jolla, CA 92037, USA.

[12] Division of Virology, Department of Microbiology and Immunology, Institute of Medical Science, University of Tokyo, 108-8639 Tokyo, Japan.

[13] The Research Center for Global Viral Diseases, National Center for Global Health and Medicine Research Institute, Tokyo 162-8655, Japan.

[14] Pandemic Preparedness, Infection and Advanced Research Center (UTOPIA), University of Tokyo, Tokyo 162-8655, Japan.

[15] These authors contributed equally

[16] Lead Contact.

*Correspondence: pcw4001@med.cornell.edu (P.C.W.)

413 E. 69th Street, Suite 1220, New York, NY 10021

Phone: +1 6469629041

Graphical abstract

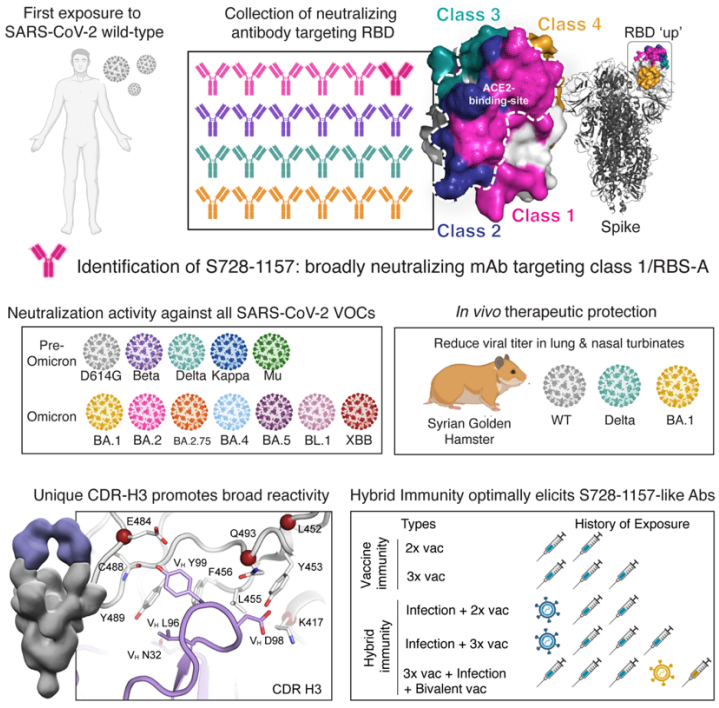

Abstract

The rapid evolution of the severe acute respiratory syndrome coronavirus 2 (SARS-CoV-2) Omicron variants has emphasized the need to identify antibodies with broad neutralizing capabilities to inform future monoclonal therapies and vaccination strategies. Herein, we identified S728-1157, a broadly neutralizing antibody (bnAb) targeting the receptor-binding site (RBS) that was derived from an individual previously infected with wildtype SARS-CoV-2 prior to the spread of variants of concern (VOCs). S728-1157 demonstrated broad cross-neutralization of all dominant variants including D614G, Beta, Delta, Kappa, Mu, and Omicron (BA.1/BA.2/BA.2.75/BA.4/BA.5/BL.1/XBB). Furthermore, S728-1157 protected hamsters against in vivo challenges with wildtype, Delta, and BA.1 viruses. Structural analysis showed that this antibody targets a class 1/RBS-A epitope in the receptor binding domain (RBD) via multiple hydrophobic and polar interactions with its heavy chain complementarity determining region region 3 (CDR-H3), in addition to common motifs in CDR-H1/CDR-H2 of class 1/RBS-A antibodies. Importantly, this epitope was more readily accessible in the open and prefusion state, or in the hexaproline (6P)-stabilized spike constructs, as compared to diproline (2P) constructs. Overall, S728-1157 demonstrates broad therapeutic potential, and may inform target-driven vaccine design against future SARS-CoV-2 variants.

Introduction

Since the start of the pandemic in December 2019, the severe acute respiratory syndrome coronavirus 2 (SARS-CoV-2) virus has led to over 660 million cases of coronavirus disease 2019 (COVID-19) and over six and a half million deaths globally. Although the rapid development and distribution of vaccines and therapeutics have curbed the impact of COVID-19 to a large extent, the emergence of circulating variants of concern (VOCs) continues to represent a major threat due to the potential for further immune evasion and enhanced pathogenicity. The D614G variant was the earliest variant to emerge and became universally prevalent thereafter. In comparison to wildtype (WT), the D614G variant exhibited increased transmissibility rather than increased pathogenicity and was therefore unlikely to reduce efficacy of vaccines in clinical trials (1). Between the emergence of D614G and October 2021, four additional significant VOCs evolved worldwide, including Alpha, Beta, Gamma, and Delta. Among these variants, Delta became a serious global threat because of its transmissibility, increased disease severity, and partial immune evasion as shown by the reduced ability of polyclonal serum and monoclonal antibodies (mAbs) to neutralize this strain (2-6). Shortly afterwards, in November 2021, the Omicron variant was identified and announced as a novel VOC. This variant possessed the largest number of mutations to date and appeared to spread more rapidly than previous strains (7, 8). Currently, there are a wide range of Omicron sublineages leading to new COVID-19 cases, with BQ.1, BQ.1.1 and XBB.1.5 becoming dominant over BA.5 and accounting for most new cases worldwide at the time of writing. The Omicron variants can escape recognition by COVID-19 vaccine-associated immunity to varying extents, thereby significantly reducing the neutralizing potency of serum antibodies from convalescent, fully mRNA-vaccinated individuals and individuals boosted with new wildtype/BA.5 bivalent mRNA vaccine (9, 10). Similarly, Omicron variants were able to escape binding of several Emergency Use-Authorization (EUA) therapeutic mAbs even though these had been previously shown to be effective against earlier VOCs (10-12). Due to the lowered neutralization against Omicron and the continued threat of future VOCs, there is an urgent need to identify broad and potent neutralizing antibodies that can protect against diverse evolving SARS-CoV-2 lineages.

In this study, we identify a potent RBD-reactive monoclonal antibody from the peripheral blood of a SARS-CoV-2 convalescent individual that effectively neutralizes Alpha, Beta, Kappa, Delta, Mu, and Omicron variants (BA.1, BA.2, BA.2.75, BA.4, BA.5, BL.1 and XBB). This mAb,

S728-1157, significantly reduce BA.1 Omicron, Delta, and wildtype viral loads in the lungs and nasal mucosa following *in vivo* challenge in hamster. S728-1157 binds the receptor binding site (RBS) that is fully exposed when the RBD on the spike is in the up conformation and uses motifs found in CDR-H1 and CDR-H2 that are common to IGHV3-53/3-66 class 1/RBS-A antibodies (13, 14), but also via extensive unique contacts with CDR-H3 to circumvent mutations in the VOCs spikes. This suggests that the rational design of future vaccine boosts covering Omicron variants should be modified to present stabilized spike in the mostly up configuration to optimally induce class 1/RBS-A mAbs that have similar CDR-H3 features.

Results

Isolation of RBD-reactive mAbs that exhibit diverse patterns of neutralization and potency

Before the spread of the Omicron lineages, we previously characterized 43 mAbs targeting distinct epitopes on the spike protein, including the N-terminal domain (NTD), RBD, and subunit 2 (S2). None of these antibodies were able to neutralize the SARS-CoV-2 variants circulating at that time (15). In this study, an additional panel of RBD-reactive mAbs were expressed from three high-responder subjects who mounted robust anti-spike IgG responses, as defined previously (16) (Table S1 and Table S3). Although the proportion of spike RBD-binding B cells was similar in high-responders as compared to mid- and low-responders (Figure 1A-C), heavy chain somatic hypermutation rates were significantly greater in the high-responder group (Figure 1D), suggesting that these subjects may have the highest potential to generate potent cross-reactive mAbs (16). These antibodies were further investigated against RBD mutants to identify their epitope classifications (17). Among 14 RBD-reactive mAbs, we identified four class 2 mAbs, two class 3 mAbs, and eight unclassified mAbs that showed little to no reduction of binding against any key RBD mutants tested (Figure 1F). To be noted, class 2, class 3 and class 4 antibodies approximately correspond to the RBS B-D, S309, and CR3022 epitopes defined in previous studies (13, 18). Class 2 and 3 RBD mAbs did not recognize a multivariant RBD mutant containing K417N/E484K/L452R/N501Y substitutions, an artificially designed RBD to include key mutations for virus escape (17, 18), nor demonstrated any cross-reactivity to the RBD of SARS-CoV-1 and Middle Eastern respiratory syndrome (MERS)-CoV (Figure 1F). Functionally, class 2 and 3 RBD mAbs potently neutralized D614G and Delta but neutralizing activity was more limited

against Beta, Kappa and Mu (Figure 1G). None of the class 2 or 3 antibodies assayed neutralized any tested Omicron variant.

In contrast, the majority of unclassified mAbs bound to the RBD multivariant and cross-reacted to the SARS-CoV-1 RBD (Figure 1F). Among these, we identified three mAbs, S451-1140, S626-161 and S728-1157, which showed high neutralization potency against D614G and cross-neutralized Beta, Delta, Kappa, Mu, and Omicron BA.1 with 99% inhibitory concentration (IC_{99}) in the range of 20-2500 ng/ml (Figure 1G). Given the broad neutralization potency of these three mAbs, in addition to the plaque assay platform, we also performed the neutralization activity against authentic BA.2.75, BL.1 (BA.2.75+R346T), BA.4, BA.5 and XBB viruses using focus reduction neutralization test (FRNT) (Figure 1G). Of these, S728-1157 displayed high neutralizing activities against the panel of Omicron variants including BA.1, BA.2, BA.4 and BA.5, with an IC_{99} up to 100 ng/ml as measured by a plaque assay. A similar scenario was observed using FRNT, where S728-1157 maintained its high neutralization activity against BA.2.75, BL.1, BA.4, BA.5 and XBB with 50% inhibitory concentration (IC_{50}) in the range of 8-300 ng/ml (Figure 1G). S451-1140 neutralized BA.1, BA.2, BA.2.75 and BL.1 potently, but not BA.4 and BA.5 as observed in both neutralization assay platforms. On the other hand, S626-161 did not demonstrate neutralizing activity against Omicron variants beyond the BA.1 variant (Figure 1G). Although S626-161 had a lower neutralization potency against the tested VOCs than the other two antibodies, it was the only mAb which showed cross-reactivity not only to SARS-CoV-1 RBD but was also able to neutralize bat coronaviruses WIV-1 and RsSHC014 (Figure 1F-G). These data suggest that S626-161 recognizes a conserved epitope that is shared between these sarbecovirus lineages but is absent in BA.2 and later strains. Additionally, compared to S728-1157 and S451-1140, S626-161 has a longer CDR-H3 that could provide an enhanced capability to recognize a highly conserved patch of residues shared across sarbecoviruses as described in a previous study (19) (Figure S1). When comparing immunoglobulin heavy (IGHV) and light chain (IGLV or IGKV) variable genes of these three mAbs with the available SARS-CoV-2 neutralizing mAbs database (13, 15, 20-27), we found that heavy chain variable genes utilized by S728-1157 (IGHV3-66), S451-1140 (IGHV3-23) and S626-161 (IGHV4-39) have been previously reported to encode several potently neutralizing SARS-CoV-2 antibodies targeting the RBD (21, 22, 28, 29). However, only S728-1157 had unique heavy and light chain variable gene pairings that have not been reported in the database (Table S3), indicating that it is not a public clonotype.

These three mAbs (S451-1140, S626-161 and S728-1157) were characterized further to determine their binding breadth against SARS-CoV-2 VOCs (Figure 2A-B). The prefusion-stabilized spike containing two-proline substitutions in the S2 subunit (2P; diproline) has been shown to be a superior immunogen compared to the wildtype spike and is the basis of several current SARS-CoV-2 vaccines, including mRNA-based vaccines (30, 31). More recently, spike protein stabilized with six prolines (6P; hexaproline) was reported to boost expression and be even more stable than the original diproline construct; as a result, it has been proposed for use in the next-generation of COVID-19 vaccines (32, 33). To determine if there are antigenicity differences between the diproline and hexaproline spike constructs, both immunogens were included in our test panel. As measured by ELISA, we found that three mAbs bound 6P-WT spike antigen to a greater extent compared to WT-2P spike (Figure 2A-B). All three mAbs showed comparable binding to the spikes of Alpha, Beta, Gamma and Delta viruses, relative to that of WT-2P (Figure 2A-B). However, the binding reactivity of these three mAbs were substantially reduced against a panel of Omicron-family antigens (Figure 2B-C). S451-1140 binding was sensitive to mutations found in BA.1 and BA.2, resulting in a large decreased in binding and a 31-fold decrease in neutralization against these variants compared with WT-2P antigen and D614G virus, respectively (Figure 2B). The sarbecovirus-cross neutralizing mAb, S626-161, also showed 1.2 to 3.5-fold reduced binding to spike BA.1 antigens, which may account for a 2-fold reduction in neutralization activity against BA.1 (Figure 1G and Figure 2B-C). For the most potent bnAb, S728-1157, binding to Omicron antigens was reduced to a lesser extent (ranging from 1.1- to 4.4-fold) compared with WT-2P spike and was unaffected in neutralizing activity (Figure 1G and Figure 2B-C). The substantial loss in these Omicron-neutralizing mAbs binding to the BA.1 spike may be alterations in its mobility and related to the tight packing of the Omicron 3-RBD-down structures and preference for one-up RBD that aid in evading antibodies as reported by previous study and references therein (34). The 2P and 6P stabilizing mutations also have differential effects in Omicron variants where all three mAbs showed over 2.8-fold increased binding to spike BA.1-6P compared with the BA.1-2P version, but only marginally increased binding to spike BA.2 and BA.4/5 6P versions compared with their 2P versions by 1.2x to 1.4x, suggesting slightly better accessibility of Omicron-neutralizing mAbs to the hexaproline versions, especially for the spike BA.1 construct. In addition to ELISA, biolayer interferometry (BLI) was used to quantify the binding rate and equilibrium constants (k_{on}, k_{off}, and K_D) of these three mAbs to a panel of spike

antigens (Figure S2). The recognition k_{on} rates of Fabs were 1.5 to 3.3-fold faster to hexaproline spikes (Figure S2B-C), showing that the antibodies bound to the 6P construct more rapidly than to 2P. This might be expected if the epitopes are more accessible on the RBD in the open state on the hexaproline spike. Except for S626-161, off-rate of the Fabs were also slower such that the overall K_D showed that S728-1157 and S451-1140 bound to the hexaproline spike with greater affinity (Figure S2B-C). The increase in binding to the hexaproline spike was even more notable for intact IgG by the 1:2 interaction model as shown by S728-1157 and S451-1140 mAbs, consistent with exposure of multiple epitopes with 6P stabilization allowing improved avidity (Figure S2A, C). Taken together, these results suggest that the epitopes targeted may be comparatively more accessible on the 6P-stabilized spike when the RBD is in the open state. Structural analyses were next performed to verify this conjecture.

Structural analysis of broadly neutralizing monoclonal antibodies

As a first approximation of epitopes bound, an ELISA competition assay was used to determine whether these three broadly neutralizing mAbs shared any overlap with our current panel of mAbs, a collection of mAbs with known epitope specificities from previous studies (15, 35, 36), and two other mAbs currently in clinical use, LY-CoV555 (Eli Lilly) (37) and REGN10933 (Regeneron) (38). The binding sites of S451-1140 and S728-1157 partially overlapped with CC12.3 (36, 39), a class 1 neutralizing antibody, and most class 2 antibodies, including LY-CoV555 and REGN10933, but not with class 3 and class 4 antibodies (Figure 3A). S626-161 shared a notable overlap in binding region with class 1 CC12.3, several class 4 antibodies including CR3022, and other unclassified antibodies, while having some partial overlap with several class 2 and one class 3 antibody (Figure 3A). Analogously, a competition BLI assay revealed that S451-1140 and S728-1157 strongly competed with one another for binding to spike WT-6P, whereas S626-161 did not (Figure S3). Overall, these data suggest S451-1140 and S728-1157 recognize similar epitopes that are distinct from S626-161.

S728-1157 was encoded by IGHV3-66 and possessed a short complementarity determining region 3 (CDR-H3). Notably, mAbs that bind the receptor binding site (RBS) in binding mode 1 (i.e. RBS-A or class 1 site), typified by CC12.1, CC12.3, B38, and C105 (13, 18, 29, 39-41), tend to use IGHV3-53 or 3-66 and are sensitive to VOC mutations (42). However, the CDR-H3 region of S728-1157 is highly distinct from other antibodies of this class, potentially accounting for its

broader activity. To understand the structural basis of broad neutralization by S728-1157 at this epitope, we solved a cryo-electron microscopy (cryo-EM) structure (Figure 3B) of IgG S728-1157 in complex with spike WT-6P-Mut7, a version of spike WT-6P possessing an interprotomer disulfide bond at C705 and C883, at ~3.3 Å global resolution (Figure S4E). Using symmetry expansion, focused classification, and refinement methods, we achieved local resolution at the RBD-Fv interface to ~4Å (Figure S4E and Table S8). A crystal structure of S728-1157 Fab was determined at 3.1 Å resolution and used to build the atomic model at the RBD-Fv interface. Our structures confirm that S728-1157 binds the RBS-A (or class 1) epitope in the RBD-up conformation (Figure 3B and Figure S4E), similar to other IGHV3-53/3-66 antibodies (Figure 3C). Steric blockage of the angiotensin converting enzyme 2 (ACE2) binding site by S728-1157 explains its high neutralization potency against SARS-CoV-2. The $_{32}$NY$_{33}$ motif and $_{53}$SGGS$_{56}$ motif (39) in S728-1157 CDR-H1 and -H2 interact with the RBD in almost the same way as CC12.3 (Figure S4B-C). However, V_H $_{98}$DY$_{99}$ in S728-1157 CDR-H3 forms more extensive interactions including both hydrophobic and polar interactions with the RBD, compared to V_H $_{98}$DF$_{99}$ in CC12.3, which may account for the broad neutralization against VOCs (Figure 3D and Tables S6-7). The diglycine V_H $_{100}$GG$_{101}$ in S728-1157 CDR-H3 may also facilitate more extensive binding compared to V_H Y$_{100}$ in CC12.3 likely due to the flexibility in the glycine residues that lead to a different conformation of the tip of the CDR-H3 loop and a relative shift of residues at $_{98}$DY$_{99}$.

Although the Omicron VOCs have extensive mutations in the RBD, most of these residues do not make interactions with or are dispensable for binding to S728-1157, as binding is still observed (Figure S4A). From our spike WT-6P-Mut7 + Fab S728-1157 model, Y505 to V_L Q31, and E484 to V_H Y99 are predicted to make hydrogen bonds (Figure S4D and Table S6), which have the potential to be disrupted by Omicron mutations Y505H and E484A. However, a Y505H mutation would still allow for a hydrogen bond with V_L Q31 and an E484A mutation would add another hydrophobic side chain near hydrophobic residues V_L Y99, F456, and Y489. These contacts may explain in part the mechanism that enables S728-1157 to retain neutralizing activity, albeit reduced against the spike BA.1 antigen (Figure 1G and Figure 2B), which in turn is possibly related to the Omicron mutations altering the conformational landscape of the spike protein (34). However, several somatically mutated residues, i.e. V_H L27, L28, R31, F58, and V_L V28 and Q31, in S728-1157 are involved in interaction with SARS-CoV-2 RBD (Figure S1 and Table S7), which

may also contribute to its broad reactivity compared to CC12.3. Overall, our structural studies revealed the basis of broad neutralization of S728-1157 that can accommodate most mutations in the SARS-CoV-2 VOCs.

S728-1157 reduces replication of SARS-CoV-2 BA.1 Omicron, Delta, and Wildtype SARS-CoV-2 in Syrian hamsters

To evaluate the protective efficacy of our broadly neutralizing mAbs, we utilized a golden Syrian hamster infection model that has been widely used for SARS-CoV-2. Hamsters received 5 mg/kg of our test mAbs or an isotype control targeting an irrelevant antigen (ebolavirus glycoprotein) via intraperitoneal injection one day post-infection with SARS-CoV-2 viruses. Lung and nasal tissues were collected at 4 days post-infection (dpi) (Figure 4A). Therapeutic administration of S728-1157 resulted in reduced titers of wildtype, BA.1 Omicron and Delta variants in both the nasal turbinates and lungs of infected hamsters (Figure 4B-D). Interestingly, the effect of S728-1157 in the lungs was dramatic, reducing wildtype and BA.1 Omicron viral loads by ~10^4 PFU, with the viral titers of the BA.1 Omicron being completely abolished (Figure 4C). In contrast to *in vitro* neutralization (Figure 1G), S451-1140 did not reduce BA.1 Omicron viral replication in lung and nasal turbinates, indicating a disconnect between in vitro neutralization and in vivo protection for this clone (Figure 4E). In comparison, S626-161 administration resulted in significant but marginal reductions in lung viral titers following wildtype and BA.1 challenge (Figure 4F-G). These data underscore that to precisely define broadly protective mAbs, evaluating protection efficacy in parallel with neutralization activity is required. Moving forward, it will be interesting to examine to what extent the protective capacity of S728-1157 is Fc-dependent. Overall, S728-1157 represents a promising mAb with broad neutralization efficacy against SARS-CoV-2 variants that is capable of dramatically reducing wildtype, Delta and BA.1 replication in vivo.

SARS-CoV-2 infection rarely elicits potent S728-1157-like cross-neutralizing mAbs

Given the cross-neutralization and prophylactic potential of S728-1157, we sought to evaluate whether S728-1157-like antibodies are commonly induced among polyclonal responses in SARS-CoV-2 patients. To assess this, we performed competition ELISAs using convalescent serum to detect anti-RBD antibody titers that could compete for binding with S728-1157 (Figure 5A). Subjects were divided into three groups based on their magnitude of antibody responses, as defined

previously (15, 16). Although high- and moderate-responders had higher titers of S728-1157-competitive serum antibodies compared to low-responders (Figure 5B), the titers were quite low across all groups suggesting that it is uncommon to acquire high levels of S728-1157-like antibodies in polyclonal serum following wildtype SARS-CoV-2 infection. In addition to S728-1157, we tested the competition of convalescent serum with other mAbs, including S451-1140 and S626-161, LY-CoV555, REGN10933, CR3022, and CC12.3. Similar to S728-1157, we observed relatively low titers of antibodies competing with S451-1140, S626-161, LY-CoV555, REGN10933 and CC12.3 in polyclonal serum from most of the convalescent individuals (Figure 5C-F, H). Nonetheless, high-responders tended to have significantly higher titers against those neutralizing mAbs than low-responders (Figure 5B-F, H). In contrast, antibodies targeting the CR3022 epitope site were more pronounced in convalescent individuals, suggesting the enrichment of class 4 RBD antibodies in polyclonal serum (Figure 5G). Notably, there was no significant difference in titers of CR3022 across the three responder groups, suggesting that CR3022-site antibodies were consistently induced during wildtype SARS-CoV-2 infection in most individuals. Interestingly, as compared to CC12.3, S728-1157 was detected at 4-fold lower levels in the serum of high-responders. Thus, despite class 1 antibodies being frequently induced by natural infection and vaccination (14, 20, 28, 29, 43-45), our data suggest that S728-1157-like antibodies that represent a subset of this class are comparatively rare.

Additionally, we examined the difference in reactivity to 2P- versus 6P-stabilized spike in our convalescent cohort sera (Figure 5I-K). We found that all three responder groups mounted anti-spike reactive antibodies against 6P-stabilized spike wildtype to a greater extent than 2P-stabilized spike wildtype, by a factor of 6 to 11-fold (Figure 5J), indicating that the major antigenic epitopes were better exhibited or stabilized on 6P-stablized antigen. Using the same samples, high and moderate responders also had lower titers of anti-spike antibodies against BA.1-2P than BA.1-6P, by 4 to 5-fold (Figure 5K). Of note, low responders had a smaller fold change in binding reactivity against spike BA.1 Omicron-2P and 6P (2-fold reduction) compared to wildtype-2P and 6P spike (11-fold reduction) (Figure 5J-K), suggesting that serum antibody against BA.1 Omicron-reactive epitopes may be more limited in low responder subjects. Overall, these data suggest that there is improved polyclonal binding induced by natural infection to 6P-stabilized spike, both for wildtype and Omicron viruses.

S728-1157-like antibodies are optimally induced in the context of hybrid immunity

Primary SARS-CoV-2 infection without vaccination has become rare in the current global setting, and several studies have been reported that SARS-CoV-2 immunity differs between individuals with specific vaccination/infection histories. As a result, we next sought to investigate which common exposures, aside from WT infection with ancestral SARS-CoV-2 alone, would effectively induce S728-1157-like antibodies in plasma from monovalent mRNA-based vaccinees with and without prior infection. We obtained the necessary biospecimen from the Protection Associated with Rapid Immunity to SARS-CoV-2 (PARIS) study cohort, which follows health care workers longitudinally since the beginning of the pandemic (46). We selected plasma samples from fully immunized (2x vacc.) study participants with and without infection as well as from boosted participants (3x vacc.) with and without infection. In addition, we also included samples from study participants who had received the bivalent mRNA vaccine (ancestral WA1/2020 plus Omicron BA.5) (Figure 6A and Table S2). The breakthrough infections in participants who had received booster vaccinations occurred at time when the Omicron lineages had displaced all other SARS-CoV-2 lineages in the New York metropolitan area. We found that double-vaccinated individuals had lowest titers of S728-1157 competitive serum antibodies among the five groups of samples tested (Figure 6B). Notably, these levels were similar to that observed for our convalescent-unvaccinated cohort (all responders; Figure 5B). In comparison, individuals with a history of natural infection, including convalescent individuals with two/three vaccine doses, and individuals that had experienced a breakthrough infection and received a bivalent booster, showed significantly higher levels of S728-1157 elicitation compared with uninfected but vaccinated individuals (Figure 6B). Although the uninfected three-dose group displayed only a non-significant increase compared to the two-dose group, paired breakdown by vaccine type indicated that homologous third doses of BNT162b2 and mRNA-1273 significantly increased S728-1157-like neutralizing antibody titers by 2.72x and 2.85x, respectively (Figure 6C-D). To note, among the participants with three total contacts to spike by any means, S728-1157-like antibody titers were 3x higher in convalescent double-vaccinees compared to infection naive triple-vaccinees, suggesting that SARS-CoV-2 infection more optimally induces this clonotype. Among hybrid immunity groups, we noted that a majority of the boosted individuals with breakthrough who received the bivalent booster vaccine dose had only marginally higher S728-1157 antibody titer compared to pre-omicron convalescent vaccinated groups, suggesting that the S728-1157 titer was

likely approaching a plateau after three exposures. We also investigated the titers of polyclonal antibodies that competed with CC12.3 and CR3022 in addition to S728-1157. All individuals exhibited relatively high titers of CC12.3 and CR3022- like antibodies independent of the number and type of exposures (Figure S5), contradictory to what we observed for S728-1157-like antibodies. Overall, these data indicate that SARS-CoV-2 infection and mRNA vaccination both contribute to S728-1157-like antibody induction, with infection playing a more dominant role in vaccinated individuals.

Finally, in comparing responses against 2P- versus 6P-stabilized spike in the mRNA-vaccination cohort, we found that most groups elicited similar levels of antibodies against both constructs. The exception to this was the uninfected triple-vaccinated group, who demonstrated statistically higher reactivity to 2P than to 6P-stabilized spike, although with only slight increases (Figure 6E). These data suggest that, in contrast to natural infection (Figure 5J-K), vaccination alone produces a polyclonal response which is more restricted to epitopes in the Spike-2P construct, in line with the Spike-2P formulation of current vaccines. Ultimately, these findings support the idea that 6P-stabilization of future SARS-CoV-2 vaccines could be of major benefit in inducing broadly protective antibody clonotypes like S728-1157.

Discussion

In this study, we identify a potent bnAb isolated from a memory B cell of an individual who had recovered from SARS-CoV-2 infection during the initial wave of the COVID-19 pandemic. This bnAb, S728-1157, maintains substantial binding reactivity and had consistent neutralizing activity against all tested SARS-CoV-2 VOC including Omicron BA.1, BA.2, BA.2.75, BL.1 (BA.2.75+R346T), BA.4, BA.5, and XBB, and was able to substantially reduce infectious viral titers following Delta and BA.1 infection in hamsters.

We found convalescent serum from our cohort contained low concentrations of antibodies that compete with S728-1157 (a class 1/ RBS-A antibody) and class 2 epitope mAbs. This suggests that S728-1157 is somewhat unique from other antibodies targeting class 1 epitopes and is infrequently induced in the RBD-specific memory B cells pool. Instead, in our cohort natural infection cohort appeared to preferably induce antibodies targeting the CR3022 (class 4) epitope; antibodies of this specificity are often cross-reactive but less potently neutralizing than RBS-targeting antibodies (14, 17). These data are complementary to our previous findings that

demonstrated that an abundance of class 3/S309 antibodies in convalescent sera may contribute to neutralizing activity against Alpha and Gamma variants, whereas a lack of class 2 antibodies may account for reduced neutralization capability against Delta (15). Notwithstanding, the breadth of activity against Omicron variants of most of these RBS-targeting antibodies (RBS-A/class 1, RBS-B,C/class 2 and RBS-D, S309/class 3) is reported to be highly limited (11, 42, 47).

The key challenge moving forward will to be determine how to improve the elicitation of broadly cross-reactive antibodies to conserved RBS-epitopes. In this regard, we observed here that individuals with hybrid immunity mounted significantly higher titers of S728-1157-like antibodies than vaccinated individuals without prior infection. Importantly, this phenomenon was noted even when the number of exposures was controlled for (i.e. in convalescent double vaccinees vs uninfected triple vaccinees), suggesting that some element of infection-associated immunity (or a vaccine formulation that can mimic this type of immunity) is important for the elicitation of this clonotype. This is consistent with experimental evidence documenting that individuals with hybrid immunity have broader antibody reactivity profiles compared to those that only have vaccination-induced or primary infection-induced immune responses (9).

The structures herein illustrated that S728-1157 bound the RBS-A/class 1 epitope in the 'up' conformation RBD. This epitope appears to be more readily accessible on 6P-stabilized spikes, which has been reported to present two RBDs in the 'up' state, as compared to 2P spikes which presents only one (30, 33, 48, 49), and to which our antibodies specific for up conformation spike show improved binding. S728-1157 was isolated after natural infection; in such contexts, the odds of inducing S728-1157-like clones are likely higher given that the RBD must be able to adopt an up conformation, even transiently, to bind to ACE2, thereby exposing this epitope. Unlike the majority of IGHV3-53/3-66 RBS-A/class 1 antibodies, S728-1157 can accommodate key mutations in VOC spikes using extensive interactions between CDR-H3 and the RBD (29, 50-52). S728-1157 also uses a different light chain (IGLV3-9) compared to other less broad antibodies such as CC12.3 (IGKV3-20), which may affect the overall binding interactions; however, our analysis indicates that there is less hydrogen bonding between the S728-1157 light chain and the RBD compared to CC12.3 (Table S7). Although most of the CDR-H3 contact residues critical for VOC cross-reactivity in this interaction are germline-encoded and not introduced by somatic mutations, several somatically mutated residues in framework regions or CDR-H1, CDR-H2, and CDR-L1 are involved in interaction with SARS-CoV-2 RBD. On the one hand, this suggests that

memory B cells encoding IGHV3-53/66 class antibodies could acquire similar degree of cross-reactivity by further affinity maturation. On the other hand, this also indicates the possibility of designing germline-targeted immunogens that target S728-1157-like naïve B cells. While it may be challenging to design vaccines that can specifically elicit S728-1157-like antibodies with select CDR-H3s capable of overcoming the VOC mutations, it is encouraging that IGHV-gene restriction is observed in other potent SARS-CoV-2 neutralizing mAbs studies (13, 15, 20-27). Alternatively, this may be also feasible through iterative immunization with optimized RBD immunogens, as has been previously reported for other pathogens (53-57).

Although many mutations have been observed in the RBS-A/class 1 antigenic site (18), with regards to the S728-1157 epitope 13/15 total RBD contact residues, and 2/3 CDR-H3-bound RBD contact residues, are conserved within Omicron and all other VOCs. This suggests that the RBD region where the S728-1157 epitope is found may include residues critical for its dynamic function and viral fitness and would therefore be less tolerant of mutations and antigenic drift than surrounding RBS-A/ class 1 site residues. If this is the case, the tendency for this particular epitope to be lost as viral variants evolve should be reduced, making characterization of S728-1157 and similar antibodies and epitopes important for variant-resistant vaccines or mAb therapeutic development.

In summary, our study identifies broadly neutralizing antibodies that may inform immunogen design for next-generation variant-proof coronavirus vaccines or serve as mAb therapeutics that are resistant to SARS-CoV-2 evolution. In particular, in terms of combined potency and breadth, S728-1157 appears to be the best-in-class antibody isolated to date. Given that this antibody binds more readily with 6P-stablization, it is predicted to be preferentially induced by 6P-stabilized recombinant spike proteins or whole virus, these findings suggest that hexaproline modification could benefit future vaccine constructs to optimally protect against future SARS-CoV-2 variants and other sarbecoviruses.

Methods

Monoclonal antibody isolation

PBMCs were isolated from leukoreduction filters and frozen as described previously (24). B cells were enriched from PBMCs via fluorescence-activated cell sorting (FACS). Cells were stained with CD19, CD3, and antigen probes conjugated oligo-fluorophore; cells of interest were

identified as $CD3^{-}CD19^{+}Antigen^{+}$. All mAbs were generated from oligo-tagged, antigen bait-sorted cells identified through single-cell RNA sequencing (RNA-seq), as described previously (15, 24). The single B cell data generated in this study have been deposited to Gene Expression Omnibus: GSE171703 and GSM5231088–GSM5231123.

Antigen-specific B cells were selected to generate mAbs based on antigen-probe intensity analyzed by JMP® Pro 15. Antibody heavy and light chain genes were synthesized by Integrated DNA Technologies (IDT) and cloned into human IgG1 and human kappa or lambda light chain expression vectors by Gibson assembly as previously described (58). The heavy and light chains of the corresponding mAb were transiently co-transfected into HEK293T cells (ATCC). After transfection for 18 h, the transfected cells were supplemented with Protein-Free Hybridoma Medium Supernatant (PFHM-II, Gibco). The supernatant containing secreted mAb was harvested at day 4 and purified using protein A-agarose beads (Thermo Fisher) as detailed previously (58). Sequences of heavy and light chains of the well-characterized antibodies were derived from Protein Data Bank (PDB), LY-CoV555 (PDB ID: 7KMG), CR3022 (PDB ID: 6W7Y) and REGN10933 (PDB ID: 6XDG) and were synthesized as described above. The CC12.3 mAb (PDB ID: 6XC4) was kindly provided by Dr. Meng Yuan at the Scripps Research Institute.

Recombinant spike protein expression

The recombinant D614G SARS-CoV-2 full-length (FL) spike, BA.2-6P, BA.4/5-6P, BQ.1-6P, BQ.1.1-6P, XBB-6P, WT RBD, single RBD mutants (R346S, K417N, K417T, G446V, L452R, S477N, F486A, F486Y, N487Q, Y489F, Q493A, Q493N, N501Y, Y505A, Y505F), combination RBD mutant (K417N/E484K/L452R/NN501Y), SARS-CoV-1 RBD and MERS-CoV RBD were generated in-house. Briefly, the recombinant antigens were expressed using Expi293F cells (Thermo Fisher Scientific). The gene of interest was cloned into mammalian expression vector (in-house modified AbVec) and transfected using ExpiFectamine 293 kit according to the manufacturer's protocol. The supernatant was harvested at day 4 after transfection and incubated with Ni-nitrilotriacetic acid (Ni-NTA) agarose (Qiagen). The purification was carried out using gravity flow column and eluted with imidazole-containing buffer as previously described (59, 60). The eluate was buffering-exchanged with PBS using Amicon centrifugal unit (Millipore). The recombinant FL spikes stabilized by 2P mutations were derived from variants B.1.1.7 Alpha, B.1.351 Beta, P.1 Gamma, B.1.617.2 Delta, BA.1, BA.2 and BA.4 Omicron were produced in the

Sather Laboratory at Seattle Children's Research Institute. The K417V, N439K, E484K RBDs and recombinant FL spike WT-2P and 6P were produced in Krammer laboratory at the Icahn School of Medicine at Mount Sinai. The SARS-CoV-2-6P-Mut7 and spike BA.1-6P were designed and produced as described in a previous study (61). The protein sequences and resources for each antigen are listed in Table S4.

Enzyme-linked immunosorbent assay (ELISA)

Recombinant SARS-CoV-2 spike/RBD proteins were coated onto high protein-binding microtiter plates (Costar) at 2 µg/ml in phosphate buffered saline (PBS) at 50 µl/well, and kept overnight at 4°C. Plates were washed with PBS containing 0.05% Tween 20 (PBS-T) and blocked with 150 µl of PBS containing 20% fetal bovine serum (FBS) for 1 h at 37°C. Monoclonal antibodies were serially diluted 3-fold starting from 10 µg/ml in PBS and incubated in the wells for 1 h at 37°C. Plates were then washed and incubated with horseradish peroxidase (HRP)-conjugated goat anti-human IgG antibody (Jackson ImmunoResearch, 1:1000) for 1 h at 37°C. After washing, 100 µl of Super AquaBlue ELISA substrate (eBioscience) was added per well. Absorbance was measured at 405nm on a microplate spectrophotometer (Bio-Rad). The assays were standardized using control antibodies with known binding characteristics in every plate, and the plates were developed until the absorbance of the control reached an optical density (OD) of 3.0. All mAbs were tested in duplicate, and each experiment was performed twice.

Serum ELISA

High protein-binding microtiter plates were coated with recombinant SARS-CoV-2 spike antigens at 2 µg/ml in PBS overnight at 4°C. Plates were washed with PBS 0.05% Tween and blocked with 200 µl PBS 0.1% Tween + 3% skim milk powder for 1 hour at room temperature (RT). Plasma samples were heat-inactivated for 1 hour at 56°C before perform serology experiment. Plasma were serially diluted 2-fold in PBS 0.1% Tween + 1% skim milk powder. Plates were incubated with serum dilutions for 2 hours at RT. The HRP-conjugated goat anti-human Ig secondary antibody diluted at 1:3000 with PBS 0.1% Tween + 1% skim milk powder was used to detect binding of antibodies. After 1-hour of incubation, plates were developed with 100 µl SigmaFast OPD solution (Sigma-Aldrich) for 10 minutes. Then, 50 µl 3M HCl was used to stop the development reaction. Absorbance was measured at 490 nm on a microplate spectrophotometer

(BioRad). End point titers were extrapolated from sigmoidal 4PL (where X is log concentration) standard curve for each sample. Limit of detection (LOD) is defined as the mean plus 3 S.D. of the O.D. signal recorded using plasma from pre-SARS-CoV-2 subjects. All calculations were performed in GraphPad Prism software (version 9.0).

Competition ELISA

To determine the target epitope classification of RBD-reactive mAbs, competition ELISAs were performed using other mAbs with known epitope binding characteristics as competitor mAbs. Competitor mAbs were biotinylated using EZ-Link sulfo-NHS-biotin (Thermo Scientific) for 2h at room temperature (RT). The excess biotin of biotinylated mAbs was removed with 7k molecular weight-cutoff (MWCO) Zeba spin desalting columns (Thermo Scientific). Plates were coated with 2 µg/ml RBD antigen overnight at 4°C. Plates were blocked with PBS–20% FBS for 2h at RT, and the 2-fold dilution of the mAbs of an undetermined class, or serum, was added, starting at 20 µg/ml of mAbs and a 1:10 dilution of serum. After antibody incubation for 2h at RT, the biotinylated competitor mAb was added at a concentration twice that of its dissociation constant (K_D) and incubated for another 2 h at RT together with the mAb or serum that was previously added. Plates were washed and incubated with 100 µl HRP-conjugated streptavidin (Southern Biotech) at a dilution of 1:1000 for 1 h at 37°C. The plates were developed with the Super AquaBlue ELISA substrate (eBioscience). To normalize the assays, the competitor biotinylated mAb was added in a well without any competing mAbs or serum as a control. Data were recorded when the absorbance of the control well reached and OD of 1.0-1.5. The percent competition between mAbs was then calculated by dividing a sample's observed OD by the OD reached by the positive control, subtracting this value from 1, and multiplying by 100. For serum, ODs were $\log_{10}$-transformed and analyzed by nonlinear regression to determine the 50% inhibition concentration (IC_{50}) values using GraphPad Prism software (version 9.0). The data were transformed to Log1P and plotted into graph representative of reciprocal serum dilution of the IC_{50} of serum dilution that can achieve 50% competition with the competitor mAb of interest. All mAbs were tested in duplicate, each experiment was performed two times independently, and values from two independent experiments were averaged.

Plaque assays

Plaque assays were performed with SARS-CoV-2 variant viruses on Vero E6/TMPRSS2 cells (Japanese Collection of Research Bioresources (JCRB)) (Table S5). Cells were cultured to achieve 90% confluency prior to being trypsinized and seeded at a density of $3x10^4$ cells/well in 96-well plates. On the following day, 10^2 plaque-forming unit (PFU) of SARS-CoV-2 variant was incubated with 2-fold-diluted mAbs for 1h. The antibody-virus mixture was incubated with Vero E6/TMPRSS2 cells for 3 days at 37°C. Plates were fixed with 20% methanol and then stained with crystal violet solution. The complete inhibitory concentrations (IC_{99}) were calculated using the log(inhibitor) versus normalized response (variable slope), performed in GraphPad Prism (version 9.0). All mAbs were tested in duplicate, and each experiment was performed twice.

Focus reduction neutralization test (FRNT)

Focus reduction neutralization test (FRNT) were used to determine neutralization activities as an additional platform beside plaque assay. Serial dilutions of serum starting at a final concentration of 1:20 will be mixed with 10^3 focus-forming units of virus per well and incubated for 1 h at 37 °C. A pooled pre-pandemic serum sample is served as a control. The antibody-virus mixture will be inoculated onto Vero E6/TMPRSS2 cells (JCRB) in 96-well plates and incubated for 1 h at 37 °C. An equal volume of methylcellulose solution was added to each well. The cells were incubated for 16 h at 37 °C and then fixed with formalin. After the formalin was removed, the cells were immunostained with a mouse monoclonal antibody against SARS-CoV-1/2 nucleoprotein [clone 1C7C7 (Sigma-Aldrich)], followed by a HRP-labeled goat anti-mouse immunoglobulin (SeraCare Life Sciences). The infected cells were stained with TrueBlue Substrate (SeraCare Life Sciences) and then washed with distilled water. After cell drying, the focus numbers were quantified by using an ImmunoSpot S6 Analyzer, ImmunoCapture software, and BioSpot software (Cellular Technology). The IC_{50} was calculated from the interpolated value from the log(inhibitor) versus normalized response, using variable slope (four parameters) nonlinear regression performed in GraphPad Prism (version 9.0).

Negative stain electron microscopy

Spike BA.1 Omicron-6P was complexed with a 0.5-fold molar excess of IgG S728-1157 and incubated for 30 mins at room temperature. The complex was diluted to 0.03 mg/ml and deposited on a glow-discharged carbon-coated copper mesh grid. 2% uranyl formate (w/v) was used to stain

the sample for 90 seconds. The negative stain dataset was collected on a Thermo Fisher Tecnai T12 Spirit (120keV, 56,000x magnification, 2.06 apix) paired with a FEI Eagle 4k x 4k CCD camera. Leginon(62) was used to automate the data collection and raw micrographs were store in the Appion database (63). Dogpicker(64) picked particles and the dataset was processed in RELION 3.0(64). UCSF Chimera(65) was used for map segmentation and figure making.

Cryo-electron microscopy and model building

SARS-CoV-2-6P-Mut7 was complexed with a 0.5-fold molar excess of IgG S728-1157 relative to trimer (3 binding sites) and incubated for 30 mins at room temperature. Grids were prepared using a Thermo Fisher Vitrobot Mark IV set to 4°C and 100% humidity. The complex, at 0.7 mg/ml, was briefly incubated with lauryl maltose neopentyl glycol (final concentration of 0.005 mM; Anatrace), deposited on a glow-discharged Quantifoil 1.2/1.3-400 mesh grid, and blotted for 3 seconds. The grid was loaded into a Thermo Fisher Titan Krios (130,000x magnification, 300 kEV, 1.045-Å pixel size) paired with a Gatan 4k x 4k K2 Summit direct electron detector. The Leginon software was used for data collection automation and resulting images were stored in the Appion database. Initial data processing was performed with cryoSPARC v3.2(66), which included CTF correction using GCTF(67), template picking, and 2D and 3D classification and refinement methods leading to a ~3.3 Å C1 global reconstruction. The particles from this reconstruction were imported into Relion 3.1 (68), subjected to C3 symmetry expansion, followed by focused 3D classifications without alignments using a mask around the antibody Fab and S-protein RBD regions of a single protomer. Classes with well-resolved density in this region were selected and subjected to additional rounds of focused classification. Refinements were performed with limited angular searches and a mask around the trimeric S-protein and a single Fab. The final set of particles reconstructed to ~3.7 Å global resolution.

Model building was initiated by rigid body docking of the x-ray structure of the Fab and a published cryo-EM model of the SARS-CoV-2 spike open state (PDB ID: 6VYB) into the cryo-EM map using UCSF Chimera (65). Manual building, mutagenesis and refinement were performed in Coot 0.9.6 (69), followed by relaxed refinement using Rosetta Relax (70). Model manipulation and validation was also done using Phenix 1.20 (71). Data collection, processing and model

building statistics are summarized in Table S8. Figures were generated using UCSF ChimeraX (72).

Crystallization and X-ray structure determination

384 conditions of the JCSG Core Suite (Qiagen) were used for crystal screening of S728-1157 Fab crystals on the robotic CrystalMation system (Rigaku) at Scripps Research. Crystallization trials were set-up by the vapor diffusion method in sitting drops containing 0.1 µl of protein complex and 0.1 µl of reservoir solution. Crystals appeared on day 14, were harvested on day 21, pre-equilibrated in cryoprotectant containing 15% ethylene glycol, and then flash cooled and stored in liquid nitrogen until data collection. Diffraction quality crystals were obtained in solution containing 0.2 M diammonium tartrate, and 20% (w/v) polyethylene glycol (PEG) 3350. Diffraction data were collected at cryogenic temperature (100 K) on Scripps/Stanford beamline 12-1 at the Stanford Synchrotron Radiation Lightsource (SSRL). The X-ray data were processed with HKL2000 (73). The X-ray structures were solved by molecular replacement (MR) using PHASER (74) with MR models for the Fabs from PDB ID: 7KN4 (75). Iterative model building and refinement were carried out in COOT (76) and PHENIX (77), respectively.

Animals and challenge viruses

To determine whether mAbs in the panel could reduce viral load *in vivo*, females, 6-8 weeks old Syrian hamsters (HsdHan®:AURA, Envigo) were intraperitoneally administered 5 mg/kg of candidate mAb 1 day after intranasal infection with 10^3 PFU of SARS-CoV-2 viruses (an early SARS-CoV-2 isolate, Delta or BA.1 Omicron). Control animals were treated with an Ebola-specific mAb (KZ52) of matched isotype. At day 4 post-infection, lung tissues and nasal turbinate were collected to evaluate viral titers by standard plaque assay on Vero E6/TMPRRSS2 cells (JCRB). The animal study was conducted in accordance with the recommendations for care and use of animals by the Institutional Animal Care and Use Committee at the University of Wisconsin under BSL-3 containment using approved protocols.

Biolayer interferometry (BLI)

To determine precise binding affinity, the dissociation constant (K_D) of each mAb was performed by biolayer interferometry (BLI) with an Octet K2 instrument (Forte Bio/Sartorius). The trimeric

spike SARS-CoV-2 and its variants were biotinylated (EZ-Link Sulfo-NHS-Biotin, ThermoFisher), desalted (Zeba Spike Desalting, ThermoFisher), and loaded at a concentration of 500 nM onto streptavidin (SA) biosensor (Forte Bio/Sartorius) for 300 s, followed by kinetic buffer (1x PBS containing 0.02% Tween-20 and 0.1% bovine serum albumin) for 60 s. The biosensor was then moved to associate with mAbs of interest (142 nM) for 300 s, followed by disassociation with the kinetic buffer for 300 s. On rate, off-rate, and K_D were evaluated with a global fit, the average of those values with high R-squared from two independent experiments were presented. Analysis was performed by Octet Data Analysis HT software (Forte Bio/Sartorius) with 1:1 fitting model for Fabs and 1:2 interacting model for IgG.

For competitive assay by BLI, streptavidin (SA) biosensor was pre-equilibrated in 1xPBS for at least 600s to bind with the biotinylated trimeric spike WT-6P and spike BA.1 Omicron-6P for 300s. The first mAb was associated on the loaded sensor for 300s, followed by the second mAb for another 300s. The final volume for all the solutions was 200 µl/well. All of the assays were performed with kinetic buffer at 30°C. Data were analyzed by Octet Data Analysis HT software (Forte Bio/Sartorius) and plotted using GraphPad Prism.

Statistics

All statistical analyses were performed using GraphPad Prism software (version 9.0). The numbers of biological repeats for experiments and specific tests for statistical significance used are described in the corresponding figure legends. P values of ≤ 0.05 were considered significant [*, $P \leq 0.05$; **, $P \leq 0.01$; ***, $P \leq 0.001$; ****, $P < 0.0001$), while P values of > 0.05 were considered as non-significant (ns)].

Study approvals

For monoclonal antibody production, human peripheral blood mononuclear cells (PBMCs) and serum of convalescent cohort were collected during the first wave of the pandemic in May 2020, before other SARS-CoV-2 variants emerged, which is outlined in **Table S1**. All studies were performed with the approval of the University of Chicago institutional review board (IRB20-0523). All participants provided prior written informed consent for the use of blood in research applications. This clinical trial was registered at ClinicalTrials.gov under identifier NCT04340050.

For serum competition ELISA, plasma from mRNA-vaccination cohort were collected from

participants in the longitudinal observational study under program PARIS (Protection Associated with Rapid Immunity to SARS-CoV-2). All PARIS participants provided written consent prior to study participation. The study was approved by the Mount Sinai Hospital Institutional Review Board (IRB-20-03374) and further details are outlined in **Table S2A** and **Table S2B**.

Author contributions

Conceptualize the study: SC, PCW. Conducting the experiments, acquiring data, analyzing data and manuscript writing: SC, PJH, HL, JLT. Performing the experiments and analyzing the data: JJM, GO, LL, DW, MK, TM, MH, NYZ, HLT, SEA, YF, AY, GS. Provided biospecimen: BM, JM, KS, VS. Manuscript editing: JJM, DW, BM, VS. Providing funding and resources: FK, DNS, ABW, IAW, YK. Supervising the work, providing critical insights, and manuscript writing: PCW, IAW, ABW, YK.

Acknowledgements

We thank the study participants from the two different studies for their generosity and willingness to help learn more about SARS-CoV-2 immune responses. We are grateful for the clinical staff at the University of Chicago Medicine Plasma Transfusion Program, headed by Dr. Maria Lucia Madariaga, for their assistance in collecting the sample and transfer to the lab. We thank Dr. Giulio Kleiner and Ms. Maria C Bermúdez-González for expert assistance, the entire PARIS study group (Gianna Y. Cai, Neko Lyttle, Annika Oostenink, Aria Rooker, CR Gleason, Christian Cognigni, Morgan van Kesteren, Jessica Nardulli, , Angela A Amoako, Dalles Andre, Johnston Tcheou, Dr. Lubbertus CF Mulder) for their hard work and the PARIS study participants for their generosity & long-term support of our translation research. We also kindly thank the University of Chicago CAT Facility (RRID SCR_017760) and the University of Chicago Genomics Facility (RRID SCR_019196) for assisting in sorting and sequencing samples. We thank Henry Tien for technical support with the crystallization robot, and Robyn Stanfield for assistance in data collection. We thank Jeffrey Copps for producing the spike proteins used for electron microscopy. We thank Bill Anderson and Charles Bowman for maintaining the microscope facility and for technical assistance. We are grateful to the staff of the Stanford Synchrotron Radiation Lightsource (SSRL) beamline 12-1 for assistance. Use of resources of the SSRL, SLAC National Accelerator Laboratory is supported by the U.S. Department of Energy, Office of Science, Office of Basic

Energy Sciences under Contract No. DE-AC02–76SF00515. Extraordinary facility operations were supported in part by the DOE Office of Science through the National Virtual Biotechnology Laboratory, a consortium of DOE national laboratories focused on the response to COVID-19, with funding provided by the Coronavirus CARES Act. The SSRL Structural Molecular Biology Program is supported by the DOE Office of Biological and Environmental Research, and by the National Institutes of Health, National Institute of General Medical Sciences (including P41GM103393).

Declaration of Interests

The University of Chicago has filed a patent application on November 11, 2021, relating to anti-SARS-CoV-2 antibodies with PCW and SC as inventors. Some of mAbs in this study are being considered for the development of therapeutic antibodies. The Icahn School of Medicine at Mount Sinai has filed patent applications relating to SARS-CoV-2 serological assays and NDV-based SARS-CoV-2 vaccines, which list FK as a coinventor. VS is listed on the serological assay patent application as co-inventor. Mount Sinai has spun out a company, Kantaro, to market serological tests for SARS-CoV-2. FK has consulted for Merck and Pfizer (before 2020) and is currently consulting for Pfizer, Seqirus, Third Rock Ventures and Avimex. The Krammer laboratory is also collaborating with Pfizer on animal models of SARS-CoV-2.

Funding information

This project was funded in part by the National Institute of Allergy and Infectious Diseases (NIAID; National Institutes of Health grant numbers U19AI082724 (PCW), U19AI109946 (PCW), U19AI057266 (PCW), the NIAID Centers of Excellence for Influenza Research and Surveillance (CEIRS) grant number HHSN272201400005C (PCW), and the NIAD Centers of Excellence for Influenza Research and Response (CEIRR) grant number 75N93019R00028 (PCW). This work was also partially supported by the NIAID Collaborative Influenza Vaccine Innovation Centers (CIVIC; 75N93019C00051, FK, PCW, IAW, ABW). YK and PCW were funded by NIAID's Pan-Coronavirus Vaccine Development Program (P01AI165077). YK was also funded by the Research Program on Emerging and Re-emerging Infectious Diseases (JP19fk0108113, JP20fk0108272, JP20fk0108301, and JP21fk0108586); the Japan Program for Infectious Diseases Research and Infrastructure (JP20wm0125002) from the Japan Agency for

Medical Research and Development (AMED); NIAID CEIRS contract HHSN272201400008C. DNS was funded by BEI/NIAID contract HHSN272201600013C. IAW and ABW were also supported by the Bill and Melinda Gates Foundation award INV-004923. Work in the Krammer laboratory was funded by the NIAID Collaborative Influenza Vaccine Innovation Centers (CIVIC) contract 75N93019C00051. In addition, this work was also partially funded by the NIAID Centers of Excellence for Influenza Research and Surveillance (CEIRS, contract # HHSN272201400008C), the NIAID Centers of Excellence for Influenza Research and Response (CEIRR, contract# 75N93021C00014) and by anonymous donors. The content is solely the responsibility of the authors and does not necessarily represent the official views of the National Institutes of Health or BMGF.

References

1. Hou YJ, Chiba S, Halfmann P, et al. SARS-CoV-2 D614G variant exhibits efficient replication ex vivo and transmission in vivo. *Science*. Dec 18 2020;370(6523):1464-1468. doi:10.1126/science.abe8499
2. Garcia-Beltran WF, Lam EC, St Denis K, et al. Multiple SARS-CoV-2 variants escape neutralization by vaccine-induced humoral immunity. *Cell*. Apr 29 2021;184(9):2523. doi:10.1016/j.cell.2021.04.006
3. Wall EC, Wu M, Harvey R, et al. Neutralising antibody activity against SARS-CoV-2 VOCs B.1.617.2 and B.1.351 by BNT162b2 vaccination. *Lancet*. Jun 19 2021;397(10292):2331-2333. doi:10.1016/S0140-6736(21)01290-3
4. Edara VV, Pinsky BA, Suthar MS, et al. Infection and vaccine-induced neutralizing-antibody responses to the SARS-CoV-2 B.1.617 variants. *N Engl J Med*. Aug 12 2021;385(7):664-666. doi:10.1056/NEJMc2107799
5. Zhou D, Dejnirattisai W, Supasa P, et al. Evidence of escape of SARS-CoV-2 variant B.1.351 from natural and vaccine-induced sera. *Cell*. Apr 29 2021;184(9):2348-2361 e6. doi:10.1016/j.cell.2021.02.037
6. Weisblum Y, Schmidt F, Zhang F, et al. Escape from neutralizing antibodies by SARS-CoV-2 spike protein variants. *Elife*. Oct 28 2020;9:e61312. doi:10.7554/eLife.61312
7. Graham F. Daily briefing: Omicron coronavirus variant puts scientists on alert. *Nature*. Nov 26 2021;doi:10.1038/d41586-021-03564-6
8. Karim SSA, Karim QA. Omicron SARS-CoV-2 variant: a new chapter in the COVID-19 pandemic. *Lancet*. Dec 11 2021;398(10317):2126-2128. 2022/01/08. doi:10.1016/S0140-6736(21)02758-6
9. Carreño JM, Alshammary H, Tcheou J, et al. Activity of convalescent and vaccine serum against SARS-CoV-2 Omicron. *Nature*. Dec 31 2021;602:682-688. doi:10.1038/s41586-022-04399-5
10. Wang Q, Iketani S, Li Z, et al. Alarming antibody evasion properties of rising SARS-CoV-2 BQ and XBB subvariants. *Cell*. Dec 14 2022;doi:10.1016/j.cell.2022.12.018
11. VanBlargan LA, Errico JM, Halfmann PJ, et al. An infectious SARS-CoV-2 B.1.1.529 Omicron virus escapes neutralization by therapeutic monoclonal antibodies. *Nat Med*. Jan 19 2022;28:490-495. doi:10.1038/s41591-021-01678-y
12. Takashita E, Kinoshita N, Yamayoshi S, et al. Efficacy of antibodies and antiviral drugs against COVID-19 Omicron variant. *N Engl J Med*. Jan 26 2022;386:995-998. doi:10.1056/NEJMc2119407
13. Yuan M, Liu H, Wu NC, Wilson IA. Recognition of the SARS-CoV-2 receptor binding domain by neutralizing antibodies. *Biochem Biophys Res Commun*. Jan 29 2021;538:192-203. doi:10.1016/j.bbrc.2020.10.012
14. Barnes CO, Jette CA, Abernathy ME, et al. SARS-CoV-2 neutralizing antibody structures inform therapeutic strategies. *Nature*. Dec 2020;588(7839):682-687. doi:10.1038/s41586-020-2852-1
15. Changrob S, Fu Y, Guthmiller JJ, et al. Cross-neutralization of emerging SARS-CoV-2 variants of concern by antibodies targeting distinct epitopes on spike. *Mbio*. Dec 21 2021;12(6):e0297521. doi:10.1128/mBio.02975-21
16. Guthmiller JJ, Stovicek O, Wang J, et al. SARS-CoV-2 infection severity is linked to superior humoral immunity against the spike. *Mbio*. Jan 19 2021;12(1):e02940-20. doi:10.1128/mBio.02940-20

17. Greaney AJ, Starr TN, Barnes CO, et al. Mapping mutations to the SARS-CoV-2 RBD that escape binding by different classes of antibodies. *Nat Commun*. Jul 7 2021;12(1):4196. doi:10.1038/s41467-021-24435-8
18. Liu H, Wilson IA. Protective neutralizing epitopes in SARS-CoV-2. *Immunol Rev*. May 22 2022;doi:10.1111/imr.13084
19. Jette CA, Cohen AA, Gnanapragasam PNP, et al. Broad cross-reactivity across sarbecoviruses exhibited by a subset of COVID-19 donor-derived neutralizing antibodies. *Cell Rep*. Sep 28 2021;36(13):109760. doi:10.1016/j.celrep.2021.109760
20. Brouwer PJM, Caniels TG, van der Straten K, et al. Potent neutralizing antibodies from COVID-19 patients define multiple targets of vulnerability. *Science*. Aug 7 2020;369(6504):643-650. doi:10.1126/science.abc5902
21. Pinto D, Park YJ, Beltramello M, et al. Cross-neutralization of SARS-CoV-2 by a human monoclonal SARS-CoV antibody. *Nature*. Jul 2020;583(7815):290-295. doi:10.1038/s41586-020-2349-y
22. Robbiani DF, Gaebler C, Muecksch F, et al. Convergent antibody responses to SARS-CoV-2 in convalescent individuals. *Nature*. Aug 2020;584(7821):437-442. doi:10.1038/s41586-020-2456-9
23. Yuan M, Liu H, Wu NC, et al. Structural basis of a shared antibody response to SARS-CoV-2. *Science*. Aug 28 2020;369(6507):1119-1123. doi:10.1126/science.abd2321
24. Dugan HL, Stamper CT, Li L, et al. Profiling B cell immunodominance after SARS-CoV-2 infection reveals antibody evolution to non-neutralizing viral targets. *Immunity*. 2021;54:1290-1303. doi:10.1016/j.immuni.2021.05.001.
25. Rogers TF, Zhao FZ, Huang DL, et al. Isolation of potent SARS-CoV-2 neutralizing antibodies and protection from disease in a small animal model. *Science*. Aug 21 2020;369(6506):956-963. doi:10.1126/science.abc7520
26. Schmitz AJ, Turner JS, Liu Z, et al. A vaccine-induced public antibody protects against SARS-CoV-2 and emerging variants. *Immunity*. Sep 14 2021;54(9):2159-2166.e6. doi:10.1016/j.immuni.2021.08.013
27. Shi R, Shan C, Duan X, et al. A human neutralizing antibody targets the receptor-binding site of SARS-CoV-2. *Nature*. Aug 2020;584(7819):120-124. doi:10.1038/s41586-020-2381-y
28. Cao Y, Su B, Guo X, et al. Potent neutralizing antibodies against SARS-CoV-2 identified by high-throughput single-cell sequencing of convalescent patients' B cells. *Cell*. Jul 9 2020;182(1):73-84.e16. doi:10.1016/j.cell.2020.05.025
29. Barnes CO, West AP, Jr., Huey-Tubman KE, et al. Structures of human antibodies bound to SARS-CoV-2 spike reveal common epitopes and recurrent features of antibodies. *Cell*. Aug 20 2020;182(4):828-842.e16. doi:10.1016/j.cell.2020.06.025
30. Corbett KS, Edwards DK, Leist SR, et al. SARS-CoV-2 mRNA vaccine design enabled by prototype pathogen preparedness. *Nature*. Oct 2020;586(7830):567-571. doi:10.1038/s41586-020-2622-0
31. Amanat F, Strohmeier S, Rathnasinghe R, et al. Introduction of two prolines and removal of the polybasic cleavage site lead to higher efficacy of a recombinant spike-based SARS-CoV-2 vaccine in the mouse model. *Mbio*. Mar 2 2021;12(2)doi:10.1128/mBio.02648-20
32. Sun W, Liu Y, Amanat F, et al. A Newcastle disease virus expressing a stabilized spike protein of SARS-CoV-2 induces protective immune responses. *Nat Commun*. Oct 27 2021;12(1):6197. doi:10.1038/s41467-021-26499-y

33. Hsieh CL, Goldsmith JA, Schaub JM, et al. Structure-based design of prefusion-stabilized SARS-CoV-2 spikes. *Science*. Sep 18 2020;369(6510):1501-1505. doi:10.1126/science.abd0826
34. Gobeil SM, Henderson R, Stalls V, et al. Structural diversity of the SARS-CoV-2 Omicron spike. *Mol Cell*. Jun 2 2022;82(11):2050-2068.e6. doi:10.1016/j.molcel.2022.03.028
35. Yuan M, Wu NC, Zhu X, et al. A highly conserved cryptic epitope in the receptor binding domains of SARS-CoV-2 and SARS-CoV. *Science*. May 8 2020;368(6491):630-633. doi:10.1126/science.abb7269
36. Rogers TF, Zhao F, Huang D, et al. Isolation of potent SARS-CoV-2 neutralizing antibodies and protection from disease in a small animal model. *Science*. Aug 21 2020;369(6506):956-963. doi:10.1126/science.abc7520
37. Starr TN, Greaney AJ, Dingens AS, Bloom JD. Complete map of SARS-CoV-2 RBD mutations that escape the monoclonal antibody LY-CoV555 and its cocktail with LY-CoV016. *Cell Rep Med*. Apr 20 2021;2(4):100255. doi:10.1016/j.xcrm.2021.100255
38. Baum A, Ajithdoss D, Copin R, et al. REGN-COV2 antibodies prevent and treat SARS-CoV-2 infection in rhesus macaques and hamsters. *Science*. Nov 27 2020;370(6520):1110-1115. doi:10.1126/science.abe2402
39. Yuan M, Liu HJ, Wu NC, et al. Structural basis of a shared antibody response to SARS-CoV-2. *Science*. Aug 28 2020;369(6507):1119-1123. doi:10.1126/science.abd2321
40. Wu NC, Yuan M, Liu H, et al. An alternative binding mode of IGHV3-53 antibodies to the SARS-CoV-2 receptor binding domain. *Cell Rep*. Oct 20 2020;33(3):108274. doi:10.1016/j.celrep.2020.108274
41. Wu Y, Wang F, Shen C, et al. A noncompeting pair of human neutralizing antibodies block COVID-19 virus binding to its receptor ACE2. *Science*. Jun 12 2020;368(6496):1274-1278. doi:10.1126/science.abc2241
42. Yuan M, Huang D, Lee CD, et al. Structural and functional ramifications of antigenic drift in recent SARS-CoV-2 variants. *Science*. Aug 13 2021;373(6556):818-823. doi:10.1126/science.abh1139
43. Yan Q, He P, Huang X, et al. Germline IGHV3-53-encoded RBD-targeting neutralizing antibodies are commonly present in the antibody repertoires of COVID-19 patients. *Emerg Microbes Infect*. Dec 2021;10(1):1097-1111. doi:10.1080/22221751.2021.1925594
44. Zhang Q, Ju B, Ge J, et al. Potent and protective IGHV3-53/3-66 public antibodies and their shared escape mutant on the spike of SARS-CoV-2. *Nat Commun*. Jul 9 2021;12(1):4210. doi:10.1038/s41467-021-24514-w
45. Wang Z, Schmidt F, Weisblum Y, et al. mRNA vaccine-elicited antibodies to SARS-CoV-2 and circulating variants. *Nature*. Apr 2021;592(7855):616-622. doi:10.1038/s41586-021-03324-6
46. Simon V, Kota V, Bloomquist RF, et al. PARIS and SPARTA: Finding the Achilles' Heel of SARS-CoV-2. *mSphere*. Jun 29 2022;7(3):e0017922. doi:10.1128/msphere.00179-22
47. Starr TN, Czudnochowski N, Liu Z, et al. SARS-CoV-2 RBD antibodies that maximize breadth and resistance to escape. *Nature*. Sep 2021;597(7874):97-102. doi:10.1038/s41586-021-03807-6
48. Walls AC, Park YJ, Tortorici MA, Wall A, McGuire AT, Veesler D. Structure, function, and antigenicity of the SARS-CoV-2 spike glycoprotein. *Cell*. Apr 16 2020;181(2):281-292.e6. doi:10.1016/j.cell.2020.02.058

49. Henderson R, Edwards RJ, Mansouri K, et al. Controlling the SARS-CoV-2 spike glycoprotein conformation. *Nat Struct Mol Biol*. Oct 2020;27(10):925-933. doi:10.1038/s41594-020-0479-4
50. Shrestha LB, Tedla N, Bull RA. Broadly-neutralizing antibodies against emerging SARS-CoV-2 variants. *Front Immunol*. 2021;12:752003. doi:10.3389/fimmu.2021.752003
51. Greaney AJ, Loes AN, Gentles LE, et al. Antibodies elicited by mRNA-1273 vaccination bind more broadly to the receptor binding domain than do those from SARS-CoV-2 infection. *Sci Transl Med*. Jun 30 2021;13(600):eabi9915. doi:10.1126/scitranslmed.abi9915
52. Reincke SM, Yuan M, Kornau HC, et al. SARS-CoV-2 Beta variant infection elicits potent lineage-specific and cross-reactive antibodies. *Science*. Feb 18 2022;375(6582):782-787. doi:10.1126/science.abm5835
53. Wrammert J, Koutsonanos D, Li GM, et al. Broadly cross-reactive antibodies dominate the human B cell response against 2009 pandemic H1N1 influenza virus infection. *J Exp Med*. Jan 17 2011;208(1):181-93. doi:10.1084/jem.20101352
54. Guthmiller JJ, Han J, Li L, et al. First exposure to the pandemic H1N1 virus induced broadly neutralizing antibodies targeting hemagglutinin head epitopes. *Sci Transl Med*. Jun 2 2021;13(596):eabg4535. doi:10.1126/scitranslmed.abg4535
55. Bajic G, Maron MJ, Adachi Y, et al. Influenza antigen engineering focuses immune responses to a subdominant but broadly protective viral epitope. *Cell Host Microbe*. Jun 12 2019;25(6):827-835.e6. doi:10.1016/j.chom.2019.04.003
56. Nachbagauer R, Feser J, Naficy A, et al. A chimeric hemagglutinin-based universal influenza virus vaccine approach induces broad and long-lasting immunity in a randomized, placebo-controlled phase I trial. *Nat Med*. Jan 2021;27(1):106-114. doi:10.1038/s41591-020-1118-7
57. Angeletti D, Kosik I, Santos JJS, et al. Outflanking immunodominance to target subdominant broadly neutralizing epitopes. *Proc Natl Acad Sci U S A*. Jul 2 2019;116(27):13474-13479. doi:10.1073/pnas.1816300116
58. Guthmiller JJ, Dugan HL, Neu KE, Lan LY, Wilson PC. An efficient method to generate monoclonal antibodies from human B cells. *Methods Mol Biol*. 2019;1904:109-145. doi:10.1007/978-1-4939-8958-4_5
59. Amanat F, Stadlbauer D, Strohmeier S, et al. A serological assay to detect SARS-CoV-2 seroconversion in humans. *Nat Med*. Jul 2020;26(7):1033-1036. doi:10.1038/s41591-020-0913-5
60. Stadlbauer D, Amanat F, Chromikova V, et al. SARS-CoV-2 seroconversion in humans: A detailed protocol for a serological assay, antigen production, and test setup. *Curr Protoc Microbiol*. Jun 2020;57(1):e100. doi:10.1002/cpmc.100
61. Torres JL, Ozorowski G, Andreano E, et al. Structural insights of a highly potent pan-neutralizing SARS-CoV-2 human monoclonal antibody. *Proc Natl Acad Sci U S A*. May 17 2022;119(20):e2120976119. doi:10.1073/pnas.2120976119
62. Suloway C, Pulokas J, Fellmann D, et al. Automated molecular microscopy: the new Leginon system. *J Struct Biol*. Jul 2005;151(1):41-60. doi:10.1016/j.jsb.2005.03.010
63. Lander GC, Stagg SM, Voss NR, et al. Appion: an integrated, database-driven pipeline to facilitate EM image processing. *J Struct Biol*. Apr 2009;166(1):95-102. doi:10.1016/j.jsb.2009.01.002
64. Voss NR, Yoshioka CK, Radermacher M, Potter CS, Carragher B. DoG Picker and TiltPicker: software tools to facilitate particle selection in single particle electron microscopy. *J Struct Biol*. May 2009;166(2):205-13. doi:10.1016/j.jsb.2009.01.004

65. Pettersen EF, Goddard TD, Huang CC, et al. UCSF Chimera-A visualization system for exploratory research and analysis. *J Comput Chem*. Oct 2004;25(13):1605-12. doi:10.1002/jcc.20084
66. Punjani A, Zhang H, Fleet DJ. Non-uniform refinement: adaptive regularization improves single-particle cryo-EM reconstruction. *Nat Methods*. Dec 2020;17(12):1214-1221. doi:10.1038/s41592-020-00990-8
67. Zhang K. Gctf: Real-time CTF determination and correction. *J Struct Biol*. Jan 2016;193(1):1-12. doi:10.1016/j.jsb.2015.11.003
68. Zivanov J, Nakane T, Forsberg BO, et al. New tools for automated high-resolution cryo-EM structure determination in RELION-3. *Elife*. Nov 9 2018;7:e42166. doi:10.7554/eLife.42166
69. Casanal A, Lohkamp B, Emsley P. Current developments in Coot for macromolecular model building of electron cryo-microscopy and crystallographic data. *Protein Sci*. Apr 2020;29(4):1069-1078. doi:10.1002/pro.3791
70. Frenz B, Ramisch S, Borst AJ, et al. Automatically fixing errors in glycoprotein structures with Rosetta. *Structure*. Jan 2 2019;27(1):134-139.e3. doi:10.1016/j.str.2018.09.006
71. Klaholz BP. Deriving and refining atomic models in crystallography and cryo-EM: the latest Phenix tools to facilitate structure analysis. *Acta Crystallogr D Struct Biol*. Oct 1 2019;75(Pt 10):878-881. doi:10.1107/S2059798319013391
72. Pettersen EF, Goddard TD, Huang CC, et al. UCSF ChimeraX: Structure visualization for researchers, educators, and developers. *Protein Sci*. Jan 2021;30(1):70-82. doi:10.1002/pro.3943
73. Otwinowski Z, Minor W. Processing of X-ray diffraction data collected in oscillation mode. *Methods Enzymol*. 1997;276:307-26.
74. McCoy AJ, Grosse-Kunstleve RW, Adams PD, Winn MD, Storoni LC, Read RJ. Phaser crystallographic software. *J Appl Crystallogr*. Aug 1 2007;40(Pt 4):658-674. doi:10.1107/S0021889807021206
75. Qiang M, Ma P, Li Y, et al. Neutralizing antibodies to SARS-CoV-2 selected from a human antibody library constructed decades ago. *Adv Sci (Weinh)*. Jan 2022;9(1):e2102181. doi:10.1002/advs.202102181
76. Emsley P, Cowtan K. Coot: model-building tools for molecular graphics. *Acta Crystallogr D Biol Crystallogr*. Dec 2004;60(Pt 12 Pt 1):2126-32. doi:10.1107/S0907444904019158
77. Adams PD, Afonine PV, Bunkoczi G, et al. PHENIX: a comprehensive Python-based system for macromolecular structure solution. *Acta Crystallogr D Biol Crystallogr*. Feb 2010;66(Pt 2):213-21. doi:10.1107/S0907444909052925
78. Montiel-Garcia D, Rojas-Labra O, Santoyo-Rivera N, Reddy VS. Epitope-Analyzer: A structure-based webtool to analyze broadly neutralizing epitopes. *J Struct Biol*. Mar 2022;214(1):107839. doi:10.1016/j.jsb.2022.107839

Figure legends

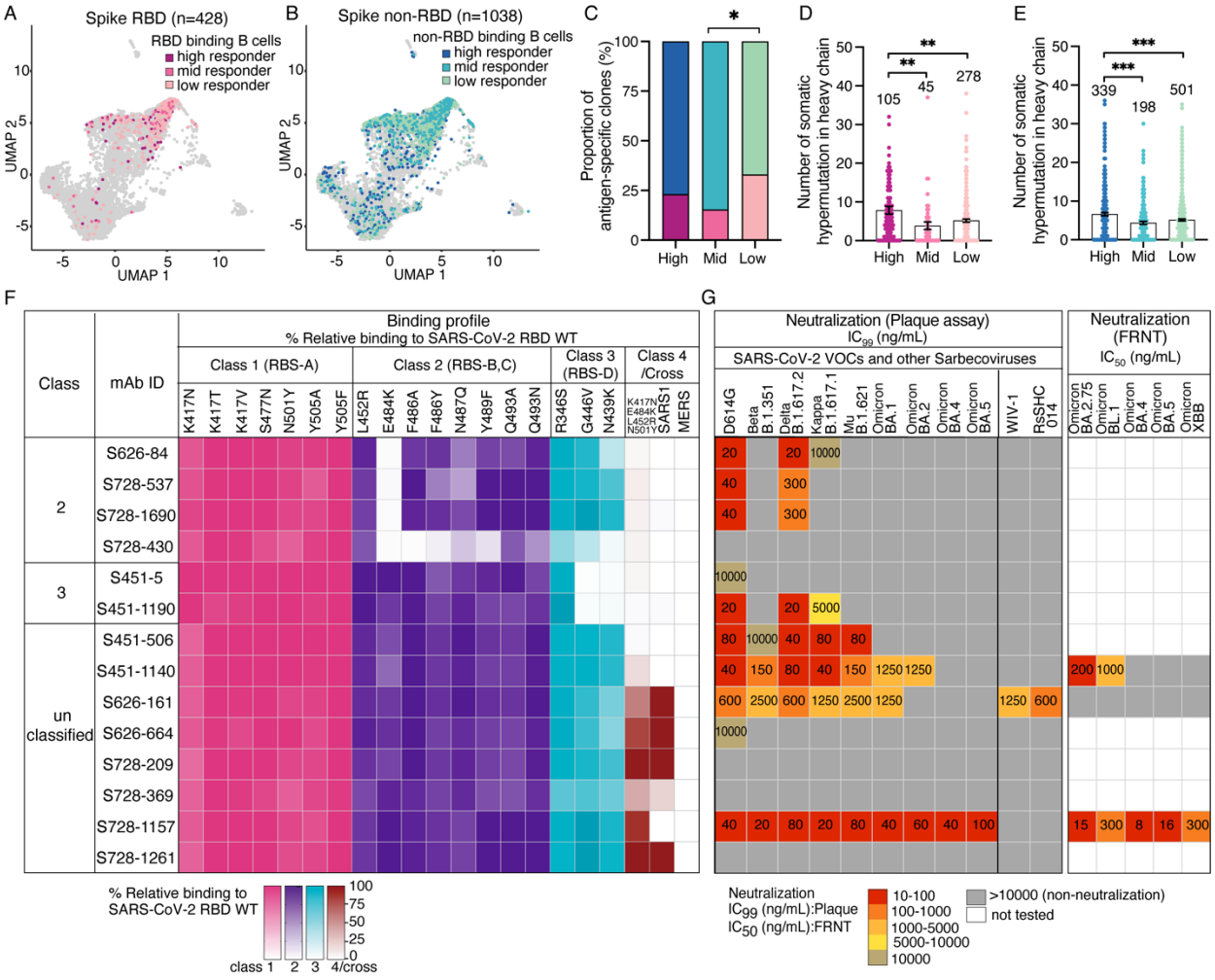

Figure 1. Characterization of RBD-reactive mAbs isolated from COVID-19 convalescent individuals. A-B, Uniform manifold approximation and projection (UMAP) of SARS-CoV-2 **(A)** spike RBD binding and **(B)** spike non-RBD binding B cells isolated from convalescent subjects that could be characterized into 3 groups (high, mid and low responder) based on their serological response against SARS-CoV-2 spike[13]. **C,** Proportion of spike non-RBD- and spike RBD-specific binding B cells representing in each responder group. Colors in **A** and **B** are representative of antigen-specific B cells from each responder group. **D-E,** Number of somatic hypermutations in the IGHV in antibodies targeting **(D)** RBD and **(E)** non-RBD. Data in **D-E** represent mean with standard deviation (SD). **F,** Binding profile of RBD-reactive mAbs against RBD mutants associated with different antibody classes, a combinatorial RBD mutant, and the RBDs of SARS-CoV-1 and MERS-CoV. Color gradients indicate relative binding percentage compared to RBD

WT. **G,** Neutralization potency measured by plaque assay (complete inhibitory concentration; IC_{99}) and focus reduction neutralization test (FRNT; half inhibitory concentration; IC_{50}) of RBD-reactive mAbs to SARS-CoV-2 variants and sarbecoviruses. The statistical analysis in **C** was determined using Tukey multiple pairwise-comparisons and in **D-E** was determined using Kruskal-Wallis with Dunn's multiple comparison test. Data in **F-G** are representative of two independent experiments performed in triplicate. Genetic information for each antibody is in **Table S3**. The SARS-CoV-2 viruses used in neutralization assay are indicated in **Table S5**.

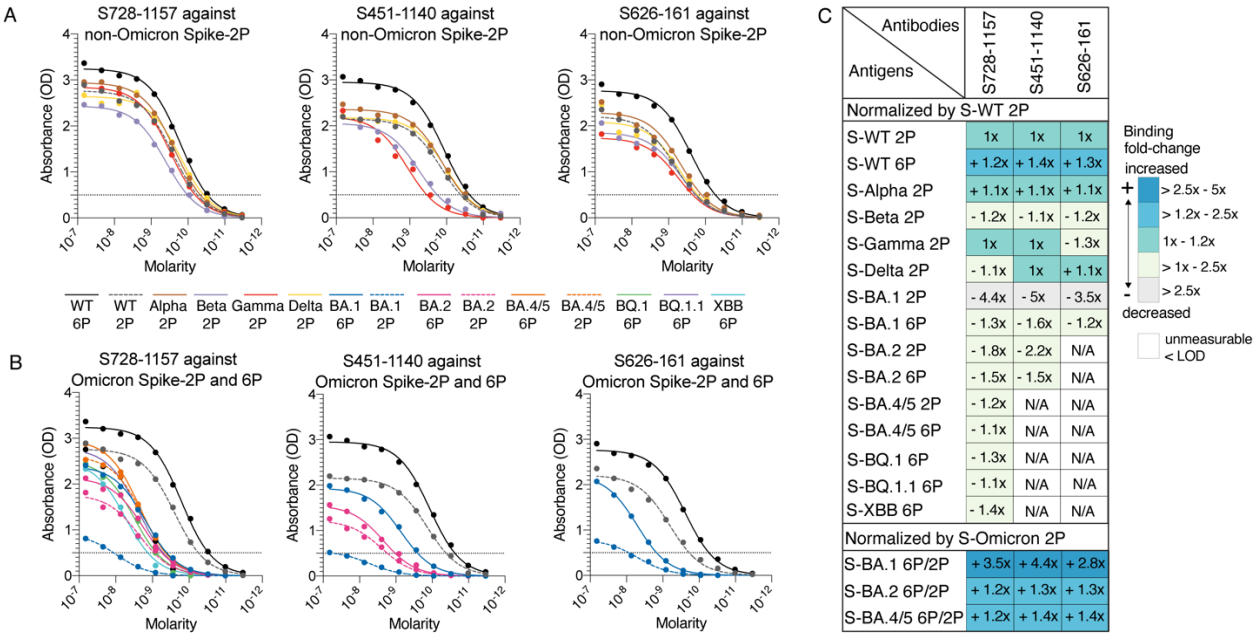

Figure 2. Binding breadth of Omicron-neutralizing mAbs. A-B, Binding profile of S728-1157, S451-1140, and S626-161 against full-length spike SARS-CoV-2 variants determined by ELISA is shown for **(A)** non-Omicron variants and **(B)** Omicron sublineages. Dashed line in **A-B** indicate the limit of detection (LOD). **C,** Heatmap represents area under curve (AUC) fold-change of neutralizing RBD-reactive mAbs against ectodomain spike SARS-CoV-2 variants relative to WT-2P and the differences of AUC fold-change between spike Omicron-2P relative to spike Omicron-6P (BA.1, BA.2 and BA4/5). Data in **A-B** are representative of three independent experiments performed in triplicate. The full-length spike SARS-CoV-2 variants used in **A-B** are detailed in **Table S4**.

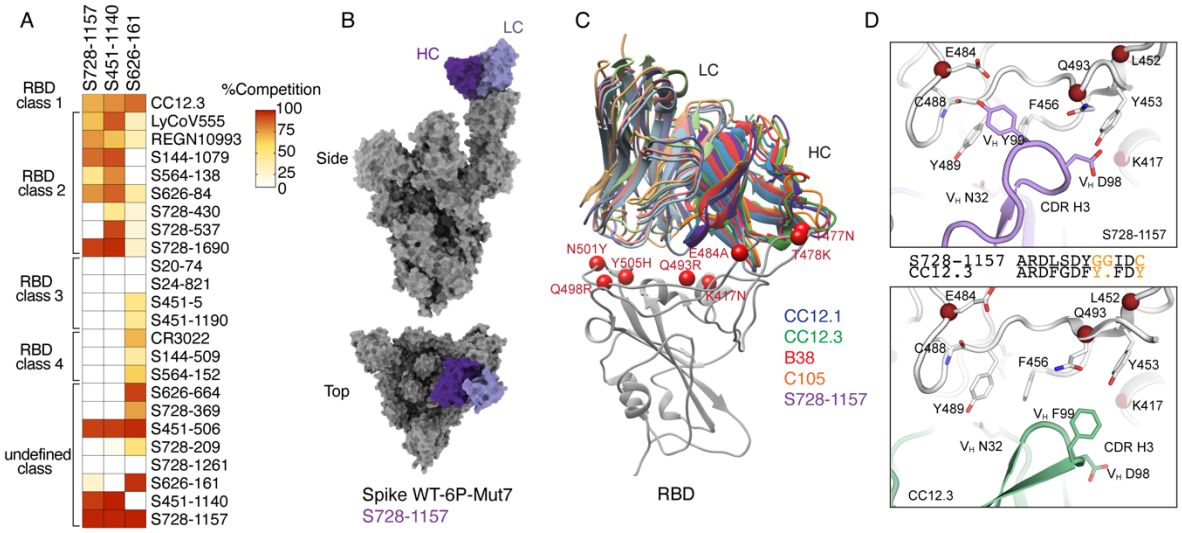

Figure 3. Mechanism of broad neutralization of S728-1157. (A) Epitope binning of broadly neutralizing RBD-reactive mAbs. Heatmap demonstrating the percentage of competition between each RBD-reactive mAb from previous studies (15, 23, 36-38) with three broadly neutralizing mAbs, S728-1157, S451-1140 and S626-161. Data are representative of two independent experiments performed in triplicate. **(B)** Surface representation of the model derived from the cryoEM map of spike WT-6P-Mut7 in complex with IgG S728-1157. The heavy chain is shown in dark purple, light chain in light purple, and the spike protein in gray. Although we observe full mAb occupancy in the cryo-EM map, only one Fv is shown here. **(C)** Structural comparison of S728-1157 to other RBS-A/class 1 antibodies such as CC12.1 (PDB ID: 6XC2, blue), CC12.3 (PDB ID: 6XC4, green), B38 (PDB ID: 7BZ5, red), and C105 (PDB ID: 6XCN, orange). The heavy chains are in a darker shade, and the light chains in a lighter shade of their respective colors. Omicron BA.1 mutations near the epitope interface are shown as red spheres. **(D)** CDR-H3 forms distinct interactions with SARS-CoV-2 RBD between S728-1157 and CC12.3. Sequence alignment of CDR-H3 of the two antibodies are shown in the middle with non-conserved residues shown in orange.

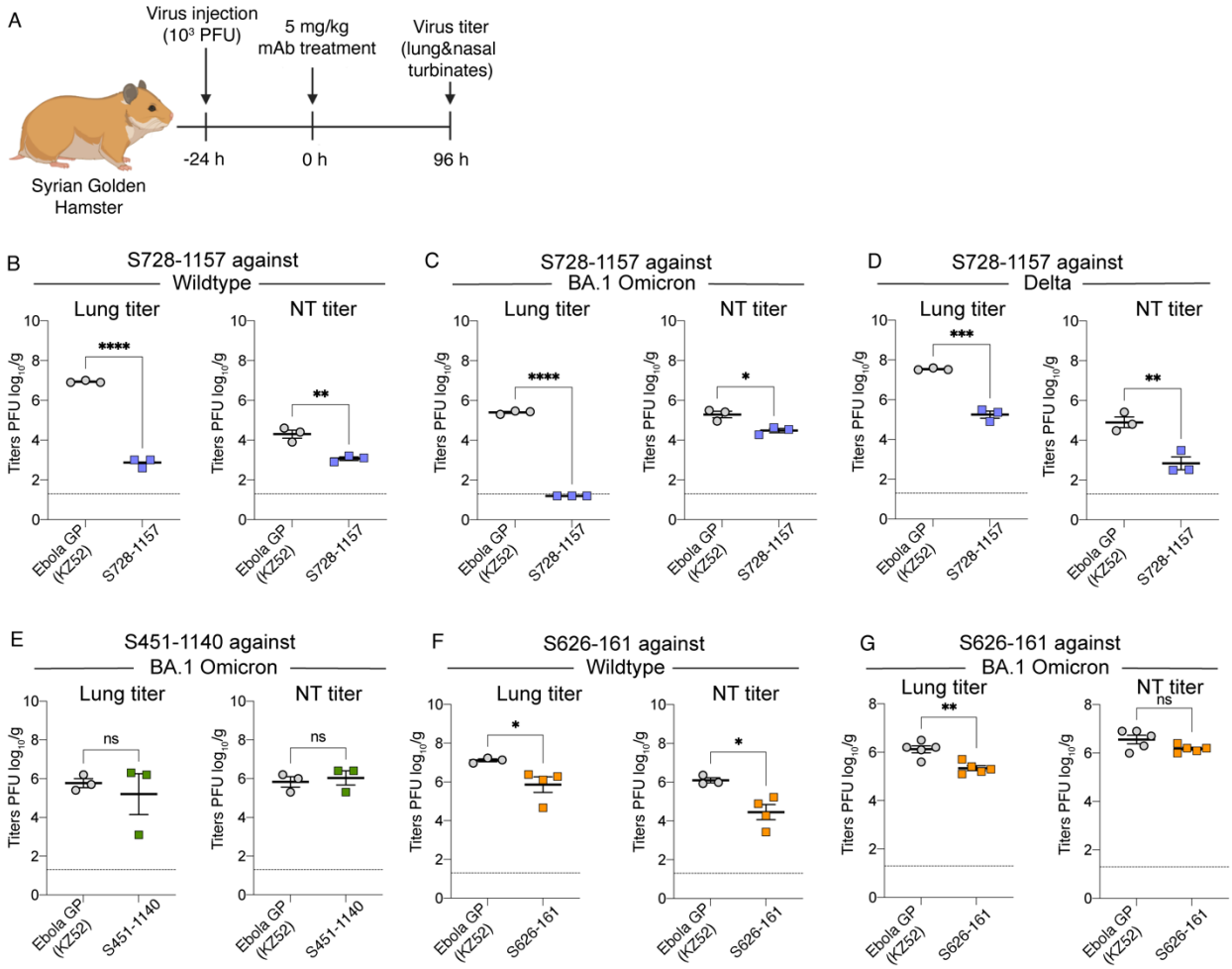

Figure 4. Protective efficacy of broadly neutralizing antibodies against SARS-CoV-2 infection in hamster. (**A**) Schematic illustrating the in vivo experiment schedule. Lung and nasal turbinate (NT) viral replication SARS-CoV-2 are shown for hamsters treated therapeutically with **(B-D)** S728-1157 (n=3) **(E)** S451-1140 (n=3) and **(F-G)** S626-161 (n=4) at day 4 post-challenge with SARS-CoV-2 compared with a control mAb, anti-Ebola surface glycoprotein (KZ52) antibody. Dashed horizontal lines represent the limit of detection (LOD) of the experiment. P-values in **(B-G)** were calculated using Unpaired t-test. The SARS-CoV-2 viruses used for infection are detailed in **Table S5**.

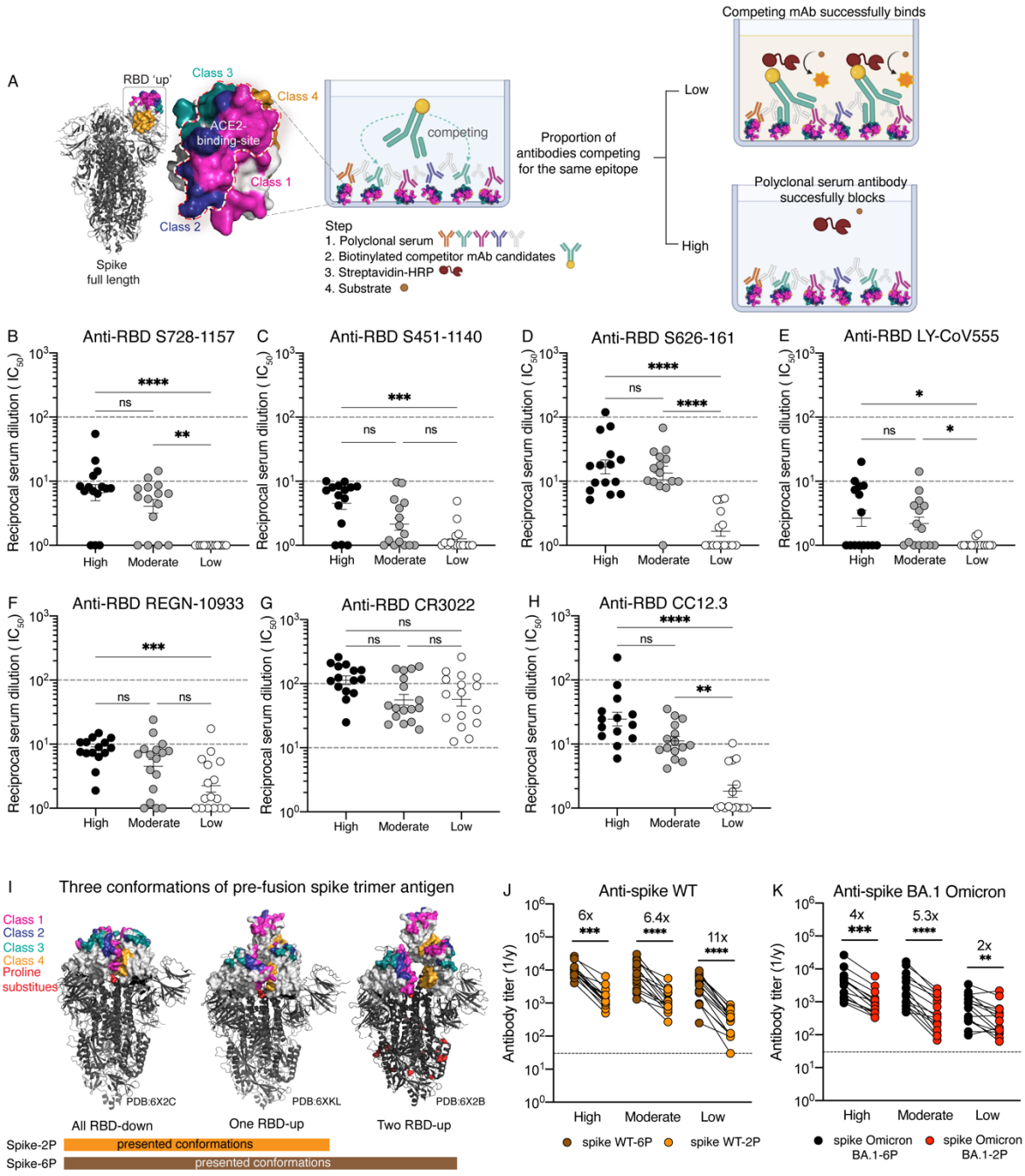

Figure 5. Convalescent serum antibody competition with broadly neutralizing RBD-reactive mAbs and comparison of serum antibody response against 6P- versus 2P-stabilized spikes. Schematic diagram for experimental procedure of serum competitive ELISA **(A)**. The model created with BioRender.com. Half-maximal inhibitory concentration (IC_{50}) of polyclonal antibody serum from convalescent individuals (high responder, n=15 donors; moderate responder, n= 16 donors; low responder, n=16 donors) that could compete with broadly neutralizing mAbs (competitor mAb): S728-1157 **(B)**, S451-1140 **(C)** and S626-161 **(D)**, as well as therapeutic mAbs

LY-CoV555 **(E)**, REGN-10933 **(F)**, non-neutralizing mAb CR3022 **(G)** and well-defined RBS-A/class 1 mAb CC12.3 **(H)**. The reciprocal serum dilutions in **B-H** are showed as Log1P of the IC_{50} of serum dilution that can achieve 50% competition with the competitor mAb of interest. The statistical analysis in **B-H** was determined using Kruskal-Wallis with Dunn's multiple comparison test. Representative three conformations of pre-fusion spike trimer antigen observed in the previous structural characterization of SARS-CoV-2 stabilized by 2P and 6P (33, 49) **(I).** Endpoint titer of convalescent sera against SARS-CoV-2 spike wildtype (WT) **(J)** and Omicron BA.1 **(K)** in two versions of spike substituted by 2P and 6P. Data in **B-H and J-K** are representative of two independent experiments performed in duplicate. Wilcoxon matched-pairs signed rank test was used to compare the anti-spike antibody titer against 2P and 6P in **J-K**. Fold change indicated in **J-K** is defined as the mean fold change.

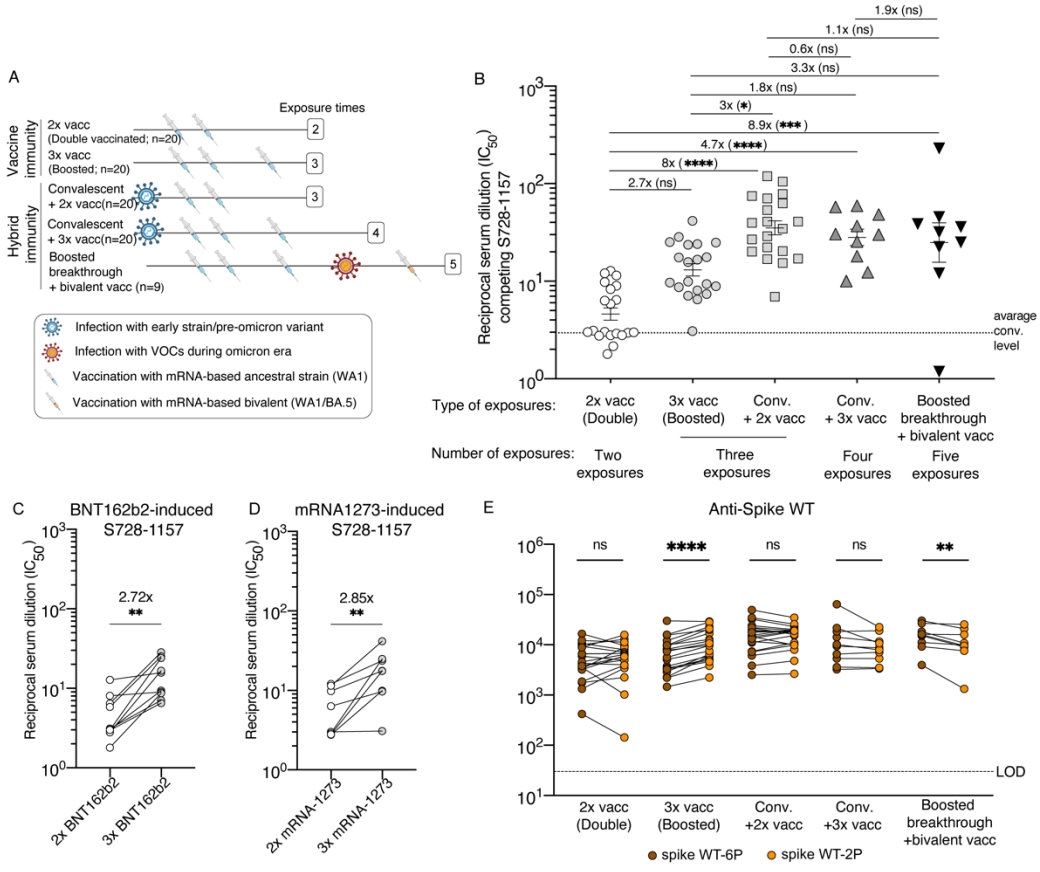

Figure 6. mRNA-vaccinated serum antibody competition with S728-1157 neutralizing RBD-reactive mAbs and comparison of serum antibody response against 6P- versus 2P-stabilized spikes. Collection of sera and exposure history from vaccine groups **(A)**. 2x vacc, double

vaccination (WA-1), (n=20 participants); 3x vacc., boosted or triple vaccination (WA-1) (n=20 participants); conv.+2x vacc., convalescent plus double vaccination (WA-1) (n=20 participants); conv.+3x vacc., convalescent plus boosted/triple vaccination (WA-1) (n=10 participants); boosted breakthrough +bivalent vacc., post-boost infection followed by bivalent vaccination (WA-1/BA.5) (n=9 participants). The model created with BioRender.com. Fold change of IC_{50} of antibody competing for binding to the S728-1157 epitope from five groups of individuals who received mRNA-based vaccine with variety type of exposure history **(B)**. Dashed line in **B** indicates average of antibody titer that was found in convalescent individual related to **Figure 4**. The statistical analysis in **B** was determined using Kruskal-Wallis with Dunn's multiple comparison test. Comparison of the kinetics of serum antibodies to the S728-1157 epitope present in a given participant after completion of the primary vaccination regimen (2x vacc.) and after boosted vaccination (3x vacc.) divided by vaccine types **(C, D)**. The connecting lines in **C** and **D** identify paired samples. Endpoint titer of mRNA-based vaccinated sera against SARS-CoV-2 spike wildtype (WT) substituted by 2P and 6P **(E)**. Dashed line in **E** indicates limit of detection (LOD) of the analysis. Wilcoxon matched-pairs signed rank test was used to compare the antibody titer in **C, D, E**. Fold change indicated in **B-D** is defined as the mean fold change. Data in **B-E** are representative of two independent experiments performed in duplicate.